IL NUOVO CIMENTO Vol. 36 C, N. 4 Luglio-Agosto 2013
DOI 10.1393/ncc/i2013-11539-9

Communications: SIF Congress 2012

# Measurement of the $t\bar{t}$ differential cross-section in $pp$ collisions at $\sqrt{s} = 7\,\mathbf{TeV}$

L. Massa

*Università di Bologna, and INFN, Sezione di Bologna - Bologna, Italy*

ricevuto il 30 Dicembre 2012

**Summary.** — Three measurements of $t\bar{t}$ differential cross section at $\sqrt{s} = 7\,\text{TeV}$ in $pp$ collisions at the Large Hadron Collider (LHC) are presented: with respect to transverse momentum, mass and rapidity of the $t\bar{t}$ system. Top pair production cross section measurements can be used to test perturbative QCD. In particular, with the high statistics collected in LHC it is possible to measure the differential cross section and look for possible deviations from the Standard Model. The results presented here have been obtained using part of the data collected by the ATLAS detector during the 2011 corresponding to an integrated luminosity of $\sim 2\,\text{fb}^{-1}$. The extension of the analysis to the full 2011 data sample ($\sim 5\,\text{fb}^{-1}$) is ongoing. The events are selected with a cut-based approach in the *single lepton plus jets* decay channel, where the lepton can be either an electron or a muon. The final background-subtracted distributions are corrected for the distortion introduced by the detector and selection effects using unfolding methods. The measurements are dominated by the systematic uncertainties and show a good agreement with the Standard Model predictions.

PACS 14.65.Ha – Top quarks.
PACS 13.38.Be – Decays of W bosons.
PACS 13.85.Hd – Inelastic scattering: many-particle final states.

## 1. – Introduction

The top quark is the last quark which has been discovered. It was first observed in 1995 by the CDF and D0 experiments at the Tevatron collider at Fermilab [1]. The world average estimates a mass $m_{top} = (173.5 \pm 0.6(stat.) \pm 0.8(sys.))\,\text{GeV}$ [2]. Studies on top mass, cross section and other proprieties are now performed at LHC, which had already produced a much larger statistics respect to the Tevatron collider and can be considered as a top-factory, producing one $t\bar{t}$ pair every few seconds at a luminosity of $10^{33}\,\text{cm}^{-2}\,\text{s}^{-1}$.

 

Being the most massive particle ever discovered, the study of the top quark is crucial to perform stringent tests on the Standard Model and search for New Physics. As a consequence of its large mass, close to the Electroweak Symmetry Breaking scale $v$, it has a large Yukawa coupling with the Higgs boson ($\lambda_{top} = \frac{\sqrt{2}m_{top}}{v} \approx 1$). Moreover, the mass of the top quark, of the $W$ boson and of the Higgs boson are strictly bounded by the corrections to the $W$ mass: hence, a precise measurement of the top quark and $W$ boson mass imposes constraints on the Higgs boson mass, also probing the internal consistency of the Standard Model. Finally, the top quark decays before hadronization ($\frac{1}{m_{top}} < \frac{1}{\Gamma_{top}} < \frac{1}{\Lambda} < \frac{m_{top}}{\Lambda^2}$), allowing precise spin studies and stringent tests of the $V-A$ interaction theory.

The $t\bar{t}$ production cross section could be used to perform tests on perturbative QCD theory, since the top quark is produced at very small distances and the perturbative expansion converges rapidly. The study of the differential cross section is a step forward towards a better understanding of the $t\bar{t}$ production process and can be performed due to the large $t\bar{t}$ statistics collected so far.

In this analysis three measurements of the $t\bar{t}$ differential cross section are performed, with respect to the mass, the transverse momentum and the rapidity of the $t\bar{t}$ system. In order to allow comparisons with the theoretical predictions and the results of the other experiments, the distortion effects due to the detector and the analysis selection are removed through unfolding techniques.

## 2. – Top pair production and decay

In a high-energy $pp$ collider, $t\bar{t}$ pairs can be produced copiously via strong interactions, but it is sizable also the production of single top quark, mainly in association with a $b$ quark, via electroweak interactions. At LHC, in $pp$ collisions at 7 TeV, the $t\bar{t}$ production is dominated by the gluon fusion process ($gg \to t\bar{t}$), which constitutes the 85% of the $t\bar{t}$ pairs, while the other 15% comes from $q\bar{q}$ annihilation.

The most precise determination of the CKM matrix element $V_{tb}$ [3] is obtained from a global fit to several measurements and imposing Standard Model constraints. According to this prediction the top quark couples almost exclusively to the bottom quark, with a $Wtb$ charged current vertex. So, in the Standard Model the top quark decays 99.8% of the times into a $b$ quark and a $W$ boson, which can decay in different ways [4]. In one third of the cases the $W$ boson decays to a $l\nu$ pair, while in the other cases it decays into a couple of quarks, ($u$,$d$) or ($c$,$s$).

Considering $t\bar{t}$ events, there will be three different channels, depending on the $W$ decay mode. If both $W$ decay hadronically we have the *full hadronic* channel; if both decay leptonically the *dileptonic* channel, while the *semileptonic* or *lepton+jets* channel is characterised by one $W$ decaying hadronically and the other leptonically:

$$t\bar{t} \to Wb + Wb \to (l\nu)b + (jj)b.$$

This analysis concentrates on the *lepton+jets* channel, where the lepton can be an electron or a muon, since it represents the best compromise in terms of statistics (with a *branching ratio* of $\sim 30\%$ [5]) and signal-to-background ratio, guaranteed by the presence of an isolated charged lepton.

## 3. – The ATLAS detector

ATLAS [6] is a multipurpose experiment which covers almost completely the whole solid angle, using a large number of sub-detectors. Particles from the interaction point moving outwards pass through an inner tracker, an electromagnetic (EM) calorimeter, an hadronic calorimeter and a muon spectrometer.

In the inner tracker, an axial magnetic field of 2 T deviates the trajectory of charged particles, which are detected in their passage through a silicon pixel detector, a silicon micro-strip tracker and a transition radiation detector.

A liquid-argon sampling-electromagnetic-calorimeter and an iron/scintillator tile hadronic calorimeter are used to measure the energy of the electrons or $\gamma$ and the hadronic jets in the barrel region. Liquid argon sampling calorimeters are also used to perform energy measurements in the forward region.

In order to detect muons, a system of tracking and trigger chambers is provided in the outer region of the detector. The trajectory and the momentum of such particles are measured using toroidal magnetic fields.

A trigger system is able to recognise events of interest, minimising dead times. The selection of the events is made using three levels of trigger, an hardware-based trigger called Level1 (L1), and two software-based triggers called Level2 (L2) and Event Filter (EF). The task of these triggers is to reduce the event rate from 40 MHz to 200 Hz.

## 4. – Particle definition and selection cuts

This analysis is performed on data collected by the ATLAS experiment [6] during proton-proton collisions at the LHC with a nominal centre-of-mass energy $\sqrt{s} = 7\,\text{TeV}$. The results presented here have been obtained using data collected in the period from March to August 2011, corresponding to an integrated luminosity of $\mathcal{L} \sim 2.05\,\text{fb}^{-1}$. The extension of the analysis to the full 2011 data sample, corresponding to an integrated luminosity of $\mathcal{L} \sim 4.7\,\text{fb}^{-1}$, is ongoing.

Events with $t\bar{t}$ decays to *lepton+jets* are characterised by an isolated high-momentum lepton, one neutrino leading to real missing-transverse-momentum multiple jets due to the presence of at least four final-state quarks, two of them coming from $b$-quark hadronization. The high-$p_T$ lepton and missing transverse energy are the signature of the leptonic decay of the $W$ boson.

Electrons are reconstructed from energy deposits in the EM calorimeter in association with one track in the inner detector. Muons are reconstructed through the combination of tracks in the muon spectrometer and in the inner detector. The reconstruction of jets is made with the anti-$k_T$ algorithm [7], using a distance parameter $\Delta R = \sqrt{(\Delta\phi)^2 + (\Delta\eta)^2} = 0.4$ (where $\phi$ is the azimuthal angle and $\eta$ is the pseudorapidity) and clusters formed starting from calorimeter cells with significant energy deposit at the EM scale, with a ratio between signal and noise greater than 4 (the noise is dependent on $\eta$ and $\phi$). Since the calorimeter is non-compensating, in order to correct the jet energy to the hadronic scale, $p_T$ and $\eta$ dependent correction factors are extracted from simulation and then validated with data [8]. The jets which are originated from bottom quarks are tagged using $b$-tagging algorithms [9], based on the long lifetime of the particles containing the bottom quark. The missing transverse energy is evaluated using the calorimeter clusters at the EM scale and then is corrected at the right energy scale of the associated physical object, while the contributions from muons are evaluated using information from the inner tracker and muon spectrometer.

Once the physical objects have been reconstructed, a set of requirements is applied in order to select events from the *lepton + jets* channel [10].

TABLE I. – *Data and background yields after selection cuts in the electron and muon channel. The likelihood cut is described in sect.* **6***, while the uncertainties are described in sect.* **8** [10].

| Channel | $e$+jets | | | $\mu$+jets | | |
|---|---|---|---|---|---|---|
| | Four jets | b-tagging | $L > -52$ | Four jets | b-tagging | $L > -52$ |
| $t\bar{t}$ | 10700±900 | 9400±800 | 7400±500 | 15800±1300 | 13900±1100 | 11100±700 |
| $W$+jets | 13000±3300 | 2200±900 | 1300±500 | 19000±5000 | 3000±1200 | 1700±700 |
| Single top | 660±50 | 530±50 | 338±32 | 950±70 | 760±80 | 490±50 |
| $Z$+jets | 1750±330 | 240±50 | 154±26 | 2200±200 | 309±34 | 192±20 |
| Diboson | 181±19 | 32±5 | 21±3 | 298±28 | 53±7 | 34±4 |
| Fake-leptons | 2000±1000 | 400±400 | 250±250 | 3400±1700 | 1100±1100 | 800±800 |
| Signal+bkg | 28000±4000 | 12800±1700 | 9500±1100 | 42000±6000 | 19200±2600 | 14400±1700 |
| Observed | 26488 | 12457 | 9187 | 42327 | 19254 | 14416 |

*Electron channel.* – The events of the $e$+jets channel are selected requiring the following conditions: one primary vertex linking more than four tracks; exactly one good electron with $E_T > 25\,\text{GeV}$ and $|\eta| < 2.47$ passing the trigger selection; absence of good muons, in order to select only electron channel events; missing transverse energy $E_T^{miss} > 30\,\text{GeV}$, due to the presence of a neutrino; the transverse mass of the leptonic $W$, $M_T(W) > 60\,\text{GeV}$, in order to reject QCD multijet contamination; at least four jets with $E_T > 25\,\text{GeV}$, of which at least one compatible with the presence of a bottom quark.

*Muon channel.* – The events of the $\mu$+jets channel are selected requiring the following conditions: one primary vertex linking more than four tracks; exactly one good muon with $p_T > 20\,\text{GeV}$ and $|\eta| < 2.5$ passing the trigger selection; absence of good electrons, in order to select only muon channel events; missing transverse energy $E_T^{miss} > 30\,\text{GeV}$, due to the presence of a neutrino; $M_T(W) + E_T^{miss} > 60\,\text{GeV}$, in order to reject QCD multijet contamination; at least four jets with $E_T > 25\,\text{GeV}$, of which at least one compatible with the presence of a bottom quark.

*Efficiency determination.* – In order to evaluate the detector acceptance and efficiencies and to estimate the systematic uncertainties, extensive Monte Carlo simulations have been performed using several generators. The top pairs and the single top processes have been simulated using *MC@NLO* [11] and *AlpGen* [12] for the hard scattering and using *Herwig* [13] for the parton showers and the hadronizations. The parton distribution functions used are the CTEQ6.6 [14].

The application of all the cuts has been studied on the Monte Carlo signal and has an efficiency of 3.8% in the electron channel and 6.3% in the muon channel. The reason of the difference between the two channels is related to the larger background in the electron channel. Due to the large cross section of the QCD multijet production, the probability of fake electrons due to misidentified hadronic jets is not negligible. So, in order to suppress such contamination, the selection cuts applied in the electron channel are harder respect to the muon channel. Data and background yields after the selection cuts are shown in table I.

## 5. – Background estimation

The selection cuts remove most of the background processes. Still there is a non negligible probability that background events, topologically very similar to the signal, pass the selection. The most important background sources which are taken into account are the $W$ and $Z$ boson production in association with multiple jets ($W$+jets and $Z$+jets), single top production, QCD multijet production, production of couple of bosons (*diboson*). The $W$+jets and $Z$+jets background processes have been simulated using *AlpGen* interfaced with the *Herwig* generator, with the CTEQ6L1 parton distribution functions [15]. Finally, the *diboson* processes have been simulated with *Herwig* using the MRST LO$^*$ parton distribution functions [16].

The QCD multijet background processes have been estimated using data-driven techniques, since their prediction is affected by a quite large uncertainty. This background is estimated through the so-called "Matrix Method" [17], which calculates the number of fake reconstructed leptons using background efficiencies that are extracted from samples dominated by multijet events. Also the overall $W$+jets normalisation is extracted with a data-driven technique called "Charge Asymmetry Method" [17], exploiting the asymmetrical cross sections of positively and negatively charged prompt leptons from $W$ decays. The contamination of all the background processes in the signal selection is estimated to be $\sim 20\%$ in both $e$+jets and $\mu$+jets channels [10].

## 6. – Reconstruction of the $t\bar{t}$ system

The reconstruction of the full $t\bar{t}$ final state is done through a kinematic fit, based on a maximum-likelihood approach [18]. The input quantities are the measured moments of the four jets and the lepton and the missing transverse energy. The kinematic fit maximises the probability of the measured quantities under the assumption of coming from $t\bar{t}$ decay, fixing the masses of $W$ boson and top quark to the world average values of $m_W = (80.385 \pm 0.015)\,\text{GeV}$ [2] and $m_{top} = (173.5 \pm 0.6 \pm 0.8)\,\text{GeV}$ [2]. The quark energies, the lepton $p_T$ and the three components of the neutrino momentum are used as fit parameters. All possible allowed combinations of reconstructed four jets, lepton and missing transverse energy are exploited in order to reconstruct the $t\bar{t}$ system. The combination that maximises the likelihood is selected. To enhance the fraction of properly reconstructed $t\bar{t}$ events, a further selection cut on the likelihood value is applied, accepting only events where $\log L > -52$.

## 7. – Unfolding

The differential distributions of the reconstructed variables are affected by the resolution of the measurements, the acceptance of the detector and the efficiency of the selection. Hence, in order to compare the reconstructed distributions with the theoretical predictions and the results from different experiments, the data must be corrected for these effects through *unfolding* procedures. Such procedures estimate the true distribution $f(x)$ of a certain physical quantity $x$, starting from the experimental measurement $y$ with its distribution $g(y)$. This estimation was performed using discrete variables $x$ and $y$, and representing $f(x)$ and $g(y)$ as histograms. In this case, the probability that an

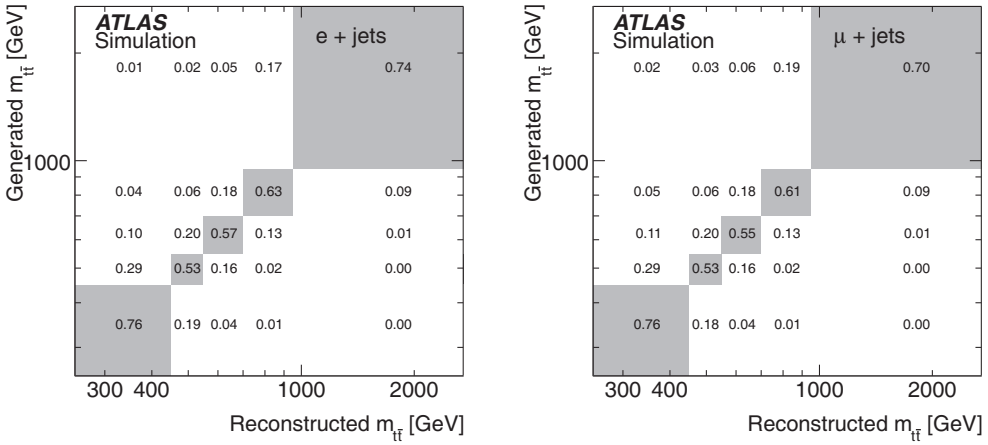


Fig. 1. – Migration matrices for the mass of the $t\bar{t}$ system in (left) e+jets and (right) $\mu$+jets channels [10].

event generated in bin $j$ is reconstructed in bin $i$ is expressed by the *migration matrix* [19]

$$\mathbf{g} = M\mathbf{f},$$

where $\mathbf{f}$ is a $n$-dimensional vector, $\mathbf{g}$ is a $m$-dimensional vector, and $M$ is a $m \times n$ matrix, related to the resolution. The $M$ matrix is generally not diagonal, because some events generated in bin $j$ could be reconstructed in bin $i \neq j$: this phenomenon is called migration. The unfolding procedure is an inverse problem, trying to solve the inverse equation with respect to the folding equation shown above. Several methods exist to handle such unfolding problem. The one used in the analysis is the so called Matrix Inversion method [19]. This method, respect to other procedures which make use of regularisation techniques in order to handle possible instability of the solutions, has the advantage to be unbiased.

*Binning choice*. – In order to avoid large migrations, the binning of each variable is optimised according to the resolution of the reconstructed variable. The result of this optimisation is that on the diagonal of the migration matrix there is about 68% of the events. The obtained migration matrix are shown in figs. 1, 2 and 3 in the case of the of mass, transverse momentum and rapidity of the $t\bar{t}$ system, respectively.

## 8. – Systematic uncertainties

The error on the differential cross-section measurement is dominated by systematics. The sources of such uncertainties are divided into two categories: *detector modelling* and *signal and background modelling*. The main contribution for the first category comes from jet related uncertainties (mainly jet energy scale and jet energy resolution) while for the second category the main sources are the modelling of the initial- and final-state radiation, the parton distribution function and the normalisation of the data-driven background.

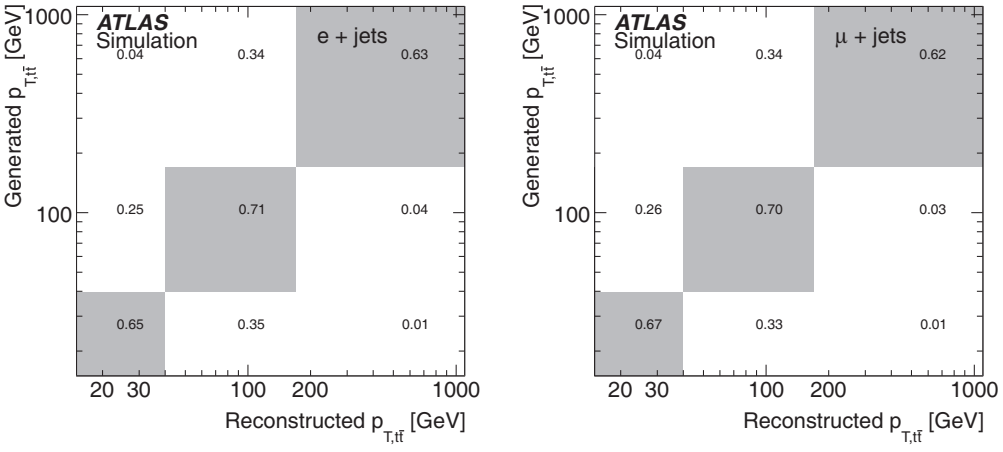


Fig. 2. – Migration matrices for the $p_T$ of the $t\bar{t}$ system in (left) e+jets and (right) $\mu$+jets channels [10].

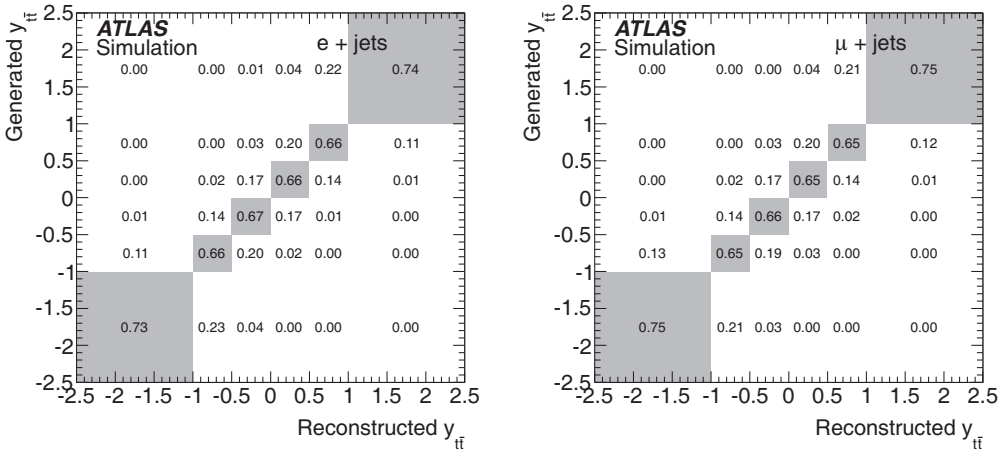


Fig. 3. – Migration matrices for the rapidity of the $t\bar{t}$ system in (left) e+jets and (right) $\mu$+jets channels [10].

## 9. – Measurement of the differential cross section

The unfolding procedure starts from the reconstructed distributions after background subtraction. The number of events in the reconstructed bin $i$ ($N_i$) is related to the number of events in the true bin $j$ through the migration matrix $M_{ij}$, derived from the $t\bar{t}$ simulation:

$$N_i = \sum_j M_{ij} A_j \sigma_j \mathcal{B} \mathcal{L} + B_i,$$

where $\mathcal{L}$ is the integrated luminosity, $A_j$ is a term containing the acceptance and the efficiency, $B_i$ is the number of background events and $\mathcal{B}$ is the branching ratio of the

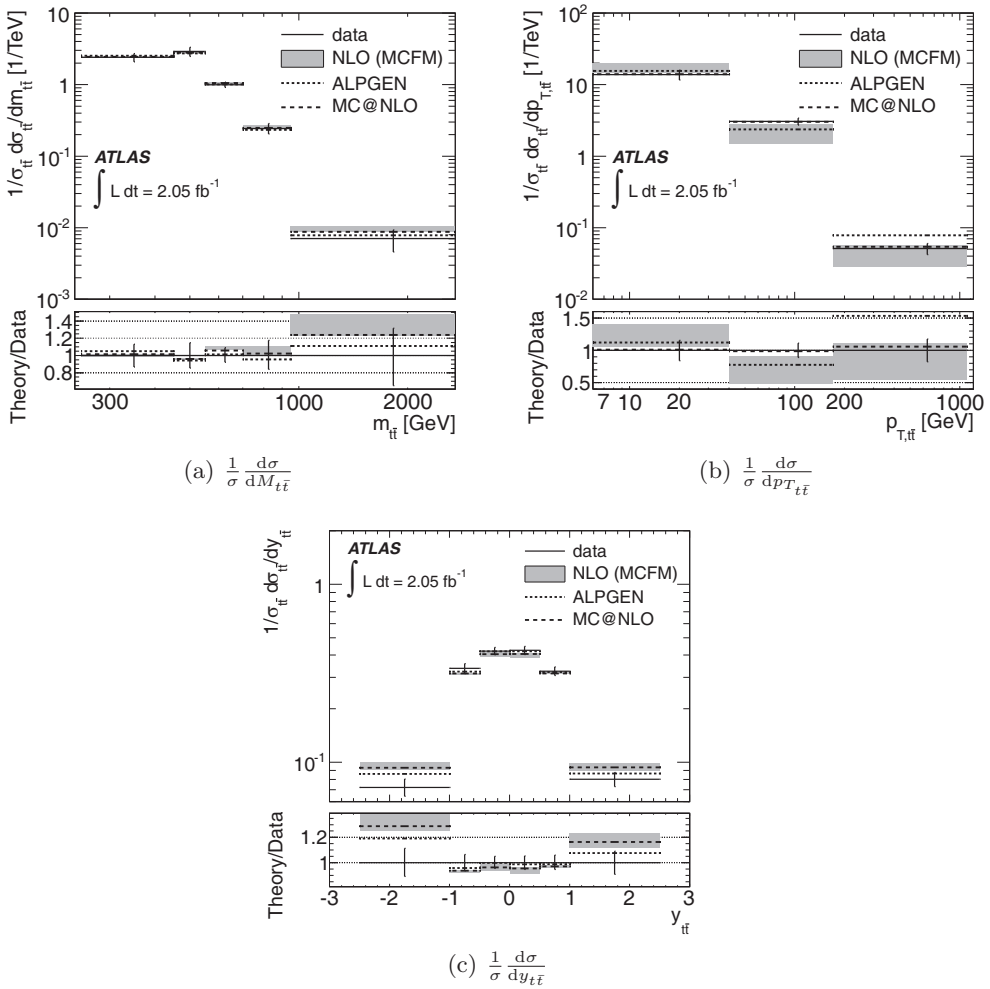


(a) $\frac{1}{\sigma}\frac{\mathrm{d}\sigma}{\mathrm{d}M_{t\bar{t}}}$ (b) $\frac{1}{\sigma}\frac{\mathrm{d}\sigma}{\mathrm{d}p_{T_{t\bar{t}}}}$

(c) $\frac{1}{\sigma}\frac{\mathrm{d}\sigma}{\mathrm{d}y_{t\bar{t}}}$

Fig. 4. – Unfolded relative differential cross section for the $M_{t\bar{t}}$, $p_{T_{t\bar{t}}}$ and $y_{t\bar{t}}$ spectrum [10].

considered decay channel. The cross section $\sigma_j$ can be extracted solving the equation

$$\sigma_j = \frac{\sum_i (M^{-1})_{ji}(N_i - B_i)}{A_j \mathcal{B}\mathcal{L}},$$

where $M^{-1}$ is estimated through the Matrix Inversion method. In the following the results for the relative differential cross sections ($\frac{1}{\sigma}\frac{\mathrm{d}\sigma}{\mathrm{d}X}$) are presented, in order to cancel out the uncertainty on the total cross section and luminosity.

## 10. – Results

The relative differential cross sections with respect to the mass, the transverse momentum and the rapidity of the $t\bar{t}$ system have been extracted from the reconstructed distributions of these kinematic quantities. The resulting relative cross sections of the

TABLE II. – *Relative differential cross-section* $\frac{1}{\sigma}\frac{\mathrm{d}\sigma}{\mathrm{d}M_{t\bar{t}}}$ *(top),* $\frac{1}{\sigma}\frac{\mathrm{d}\sigma}{\mathrm{d}p_{T_{t\bar{t}}}}$ *(middle) and* $\frac{1}{\sigma}\frac{\mathrm{d}\sigma}{\mathrm{d}y_{t\bar{t}}}$ *(bottom) measured in the e+jets, μ+ jets and the combined lepton+jets channel* [10].

| $M_{t\bar{t}}$ [GeV] | $\frac{1}{\sigma}\frac{\mathrm{d}\sigma}{\mathrm{d}M_{t\bar{t}}}$ [1/TeV] | | |
|---|---|---|---|
| | e+ jets | $\mu$+jets | lepton+jets |
| 250–450 | 2.2±0.4 | $2.5^{+0.3}_{-0.4}$ | $2.4^{+0.3}_{-0.4}$ |
| 450–550 | 3.3±0.6 | $2.8^{+0.5}_{-0.4}$ | 2.9±0.4 |
| 550–700 | 0.9±0.1 | 1.1±0.1 | 1.0±0.1 |
| 700–950 | 0.28±0.06 | $0.23^{+0.05}_{-0.04}$ | 0.24±0.04 |
| 950–2700 | 0.007±0.003 | 0.008±0.004 | 0.007±0.003 |

| $p_{T_{t\bar{t}}}$ [GeV] | $\frac{1}{\sigma}\frac{\mathrm{d}\sigma}{\mathrm{d}p_{T_{t\bar{t}}}}$ [1/TeV] | | |
|---|---|---|---|
| | e+ jets | $\mu$+jets | lepton+jets |
| 0–40 | 14±2 | 14±2 | 14±2 |
| 40–170 | 3.0±0.4 | 3.1±0.3 | 3.0±0.3 |
| 170–1100 | 0.050±0.010 | 0.051±0.008 | 0.051±0.008 |

| $y_{t\bar{t}}$ | $\frac{1}{\sigma}\frac{\mathrm{d}\sigma}{\mathrm{d}y_{t\bar{t}}}$ | | |
|---|---|---|---|
| | e+ jets | $\mu$+jets | lepton+jets |
| −2.5–(−1) | 0.070±0.010 | 0.077±0.009 | 0.072±0.008 |
| −1–(−0.5) | 0.32±0.03 | 0.35±0.03 | 0.34±0.02 |
| −0.5–0 | 0.43±0.03 | 0.41±0.02 | 0.42±0.02 |
| 0–0.5 | 0.42±0.04 | 0.43±0.02 | 0.42±0.02 |
| 0.5–1 | 0.34±0.03 | 0.31±0.02 | 0.32±0.02 |
| 1–2.5 | 0.080±0.010 | 0.083±0.007 | 0.080±0.007 |

$e$+jets and $\mu$+jets channels are combined using a weighted mean which includes the full covariance matrix between the channels. The resulting spectra of the unfolded relative differential cross section are shown in figs. 4(a), (b) and (c) for $\frac{1}{\sigma}\frac{\mathrm{d}\sigma}{\mathrm{d}M_{t\bar{t}}}$, $\frac{1}{\sigma}\frac{\mathrm{d}\sigma}{\mathrm{d}p_{T_{t\bar{t}}}}$ and $\frac{1}{\sigma}\frac{d\sigma}{dy_{t\bar{t}}}$, respectively.

The measured distributions are compared with the predictions from *MC@NLO*, *AlpGen* and *MCFM* [20]. *MC@NLO* includes full NLO matrix element calculation, while *AlpGen* is a tree level LO generator which allows for multi-parton final states; both generators include the parton shower. Also *MCFM* gives a NLO prediction, but differently from *MC@NLO*, the parton shower is not included. The unfolded distributions, represented by the black dots, are in good agreement with the theoretical predictions, as shown by the ratio between the unfolded data and the *MCFM* prediction in the lower part of the plots. Also in the case of $y$, where there are some differences between data and prediction at large absolute value of the rapidity, the values agree with the theoretical predictions within $3\sigma$ uncertainties. The values of the relative differential cross sections with respect to the mass, the transverse momentum and the rapidity of the $t\bar{t}$ system in the different bins are listed in table II for the electron channel, the muon channel and the combined channel.

## 11. – Conclusions

The unfolded relative differential distributions of the mass, the transverse momentum and the rapidity of the $t\bar{t}$ system have been evaluated and compared with the theoretical predictions obtained using *MC@NLO*, *AlpGen* and *MCFM*. The results of this analysis, which are in good agreement with the Standard Model predictions, can be considered a step forward towards a better knowledge of the top quark production mechanism and give a relevant contribution in testing precisely the perturbative QCD predictions. The analysis is going to be extended to the full data sample collected during the 2011 LHC run, corresponding to an integrated luminosity of $4.7\,\mathrm{fb}^{-1}$. The updated analysis will improve the precision of the measurement since the continuous calibration studies and the better understanding of the detector response allowed to considerably reduce the systematic uncertainties.

REFERENCES


[1] Abe F. *et al.* (CDF Collaboration), *Phys. Rev. Lett.*, **74** (1995) 2626, Abachi S. *et al.* (D0 Collaboration), *Phys. Rev. lett.*, **74** (1995) 2422.
[2] Beringer J. *et al.* (Particle Data Group), *Phys. Rev. D*, **86** (2012) 010001.
[3] Cabibbo N., *Phys. Rev. Lett.*, **10** (1963) 531, Kobayashi M. and Maskawa T., *Prog. Theor. Phys.*, **49** (1973) 652.
[4] Barisonzi M., *Top Physics at ATLAS*, arXiv:hep-ex/0508008v1 (2005).
[5] The ATLAS Collaboration, *ATLAS Detector and Physics Performance: Technical Design Report II*, *CERN/LHCC*, **99-15** (1999) .
[6] The ATLAS Collaboration, *JINST*, **3** (2008) S08003.
[7] Cacciari M. and Salam G., *Dispelling the $n^3$ myth for the kt jet-finder*; arXiv:hep-ph/0512210v2 (2005).
[8] The ATLAS Collaboration, *Eur. Phys. J. C*, **73** (2013) 2304; arXiv:hep-ex/1112.6426 (2011).
[9] The ATLAS Collaboration, *Commissioning of the Atlas high-performance b-tagging algorithms in the 7 TeV collision data*, *ATLAS-CONF*, **2011-102** (2011) .
[10] The ATLAS Collaboration, *Measurements of top quark pair relative differential cross-sections with ATLAS in pp collisions at $\sqrt{s} = 7$ TeV*, arXiv:hep-ex/1207.5644 (2012).
[11] Frixione S., Nason P. and Webber B. R., *JHEP*, **08** (2003) 007; arXiv:hep-ph/0305252 (2003).
[12] Mangano M. L. *et al.*, *JHEP*, **07** (2003) 001; arXiv:hep-ph/0206293 (2003).
[13] Corcella G. *et al.*, *JHEP*, **01** (2001) 010; arXiv:hep-ph/0011363 (2001).
[14] Pavel M., Nadolsky *et al.*, *Phys. Rev. D*, **78** (2008) 013004; arXiv:hep-ph/0802.0007 (2008).
[15] Pumplin J. *et al.*, *JHEP*, **07** (2002) 012; arXiv:hep-ph/0201195 (2002).
[16] Sherstnev A. and Thorne R., *Eur. Phys. J. C*, **55** (2008) 553; arXiv:hep-ph/0711.2473 (2008).
[17] The ATLAS Collaboration, *Expected performance of the ATLAS experiment - detector, trigger and physics*, *CERN-OPEN*, **2008-020** (2008) .
[18] The ATLAS Collaboration, *Measurement of the charge asymmetry in top quark pair production in pp collisions at $\sqrt{s} = 7$ TeV using the ATLAS detector*, arXiv:hep-ex/1204.0952 (2012).
[19] Bobel V., *Unfolding methods in high energy physics experiments, Proceedings of the 1984 CERN School of Computing*, *CERN*, **85-09** (1985) .
[20] Campbell J. M. and Ellis R. K., *MCFM for the Tevatron and the LHC*, arXiv:hep-ph/1007.3492 (2010).